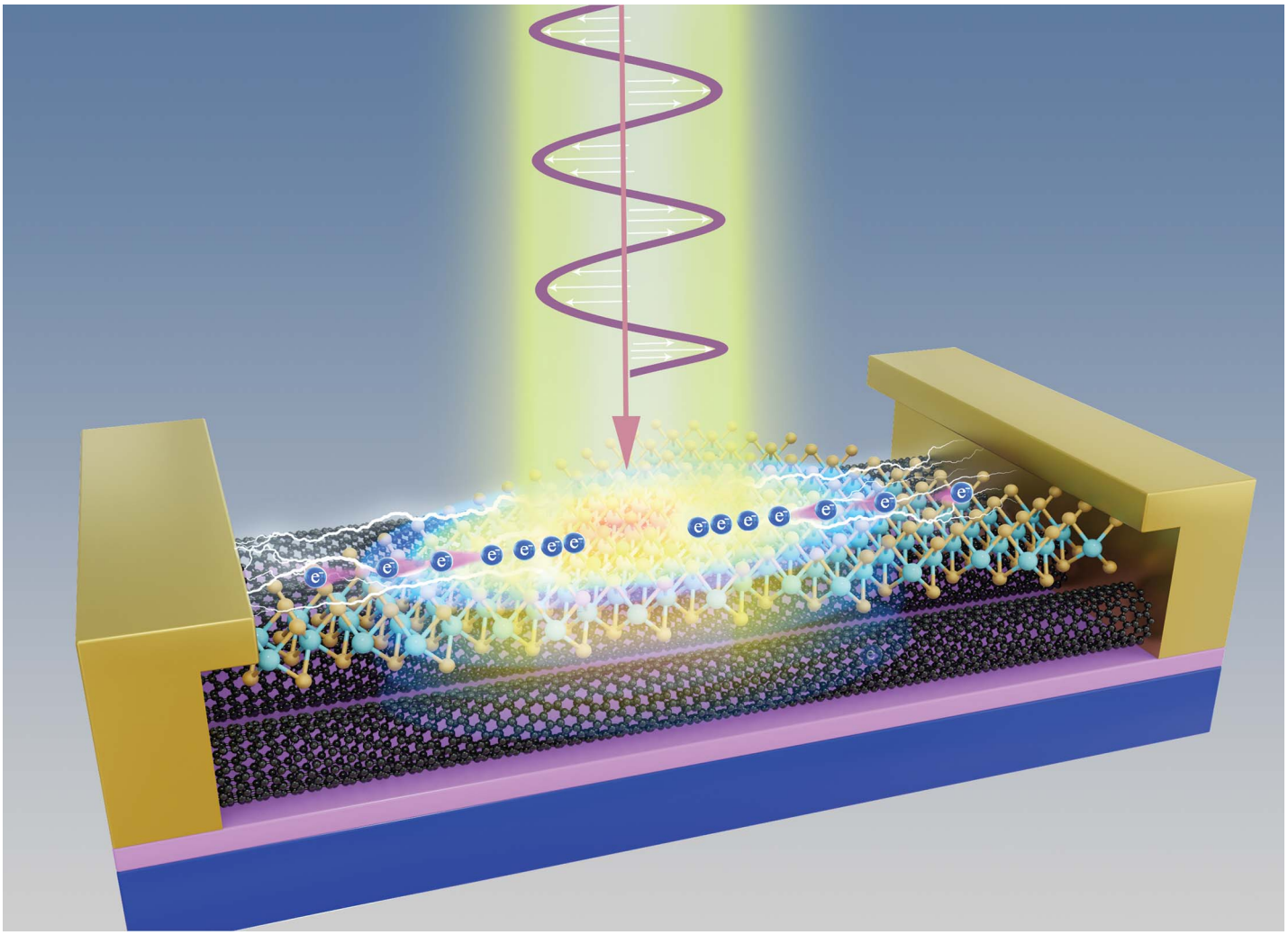

Showcasing research from Professor Cheng-Yan Xu's laboratory, School of Materials Science and Engineering, Harbin Institute of Technology, Shenzhen, China.

A polarization-sensitive photothermoelectric photodetector based on mixed-dimensional SWCNT–MoS_2 heterostructures

Xu and co-workers synthesized atomically thin MoS_2 monolayers on highly aligned metallic single-walled carbon nanotube (SWCNT) films. The photo-induced temperature gradient in SWCNT-MoS_2 hybrid films drives carrier diffusion to generate photocurrent via strong photothermoelectric (PTE) effect, and a polarization-sensitive PTE photodetector was demonstrated.

As featured in:

See Jing-Kai Qin, Cheng-Yan Xu *et al.*, *Nanoscale Adv.*, 2022, **4**, 5290.

ROYAL SOCIETY OF CHEMISTRY

rsc.li/nanoscale-advances

Registered charity number: 207890

Nanoscale Advances

ROYAL SOCIETY OF CHEMISTRY

PAPER

View Article Online
View Journal | View Issue

Cite this: *Nanoscale Adv.*, 2022, **4**, 5281

Cytotoxic sub-nanometer aqueous platinum clusters as potential antitumoral agents†

Rossella Greco,‡[a] Guillermo García-Lainez,‡[b] Judit Oliver-Meseguer,[a] Carlo Marini,[c] Irene Domínguez,[d] Miguel López-Haro,[e] Juan Carlos Hernández-Garrido,[e] José Pedro Cerón-Carrasco,[f] Inmaculada Andreu*[bg] and Antonio Leyva-Pérez*[a]

Received 17th August 2022
Accepted 9th October 2022

DOI: 10.1039/d2na00550f

rsc.li/nanoscale-advances

Ligand-free sub-nanometer metal clusters (MCs) of Pt, Ir, Rh, Au and Cu, are prepared here in neat water and used as extremely active (nM) antitumoral agents for HeLa and A2870 cells. The preparation just consists of adding the biocompatible polymer ethylene-vinyl alcohol (EVOH) to an aqueous solution of the corresponding metal salt, to give liters of a MC solution after filtration of the polymer. Since the MC solution is composed of just neat metal atoms and water, the intrinsic antitumoral activity of the different sub-nanometer metal clusters can now fairly be evaluated. Pt clusters show an IC_{50} of 0.48 μM for HeLa and A2870 cancer cells, 23 times higher than that of cisplatin and 1000 times higher than that of Pt NPs, and this extremely high cytotoxicity also occurs for cisplatin-resistant (A2870 cis) cells, with a resistance factor of 1.4 (IC_{50} = 0.68 μM). Rh and Ir clusters showed an IC_{50} ~ 1 μM. Combined experimental and computational studies support an enhanced internalization and cytotoxic activation.

Introduction

Cancer is one of the most prevalent diseases and is the second leading cause of death worldwide. In this context, ovarian cancer is the seventh most common type of cancer in women. Generally, cancer therapy includes surgery, chemotherapy, and/or radiotherapy; however, they are invasive and present important side effects.[1] Thus, the development of new targeted therapies for ovarian cancer could revolutionize treatment and significantly boost survival rates for women with this disease.[2]

In medicinal inorganic chemistry, the use of metallic complexes in cancer treatment is a burning topic, where cisplatin [$PtCl_2(NH_3)_2$] represents the principal drug in widespread clinical studies[3] and moreover, it appears in the essential medicine World Health Organization's List.[4] However, it shows side effects, including cell-death resistance generated during prolonged treatments.[5] Besides, as indicated in Fig. 1, cisplatin costs >200 € per gram, which is a lot more expensive than the public health budget.

In the last few decades, nanotechnology has received special attention because it offers challenging opportunities to improve

[a]*Instituto de Tecnología Química (UPV-CSIC) Universitat Politècnica de València-Consejo Superior de Investigaciones Científicas, Avda. de los Naranjos s/n, 46022 Valencia, Spain. E-mail: anleyva@itq.upv.es*

[b]*Instituto de Investigación Sanitaria (IIS) La Fe, Unidad Mixta de Investigación UPV/IIS La Fe, Hospital Universitari i Politècnic La Fe, Avenida de Fernando Abril Martorell 106, 46026 Valencia, Spain. E-mail: iandreur@qim.upv.es*

[c]*CELLS-ALBA Synchrotron, E-08290 Cerdanyola del Vallès, Barcelona, Spain*

[d]*Department of Chemistry and Physics, University of Almeria, Agrifood Campus of International Excellence, ceiA3, 04120 Almeria, Spain*

[e]*Departamento de Ciencia de los Materiales e Ingeniería Metalúrgica y Química Inorgánica, Facultad de Ciencias, Universidad de Cádiz, Campus Río San Pedro, 11510 Puerto Real, Cádiz, Spain*

[f]*Centro Universitario de la Defensa, Academia General del Aire. Universidad Politécnica de Cartagena. C/ Coronel López Peña S/N, Santiago de La Ribera, 30720, Murcia, Spain*

[g]*Departamento de Química, Universitat Politècnica de València Camino de Vera s/n, 46022 València, Spain*

† Electronic supplementary information (ESI) available: Experimental details, Fig. S1–S28 and Table S1. See DOI: https://doi.org/10.1039/d2na00550f

‡ These authors equally contributed to the work.

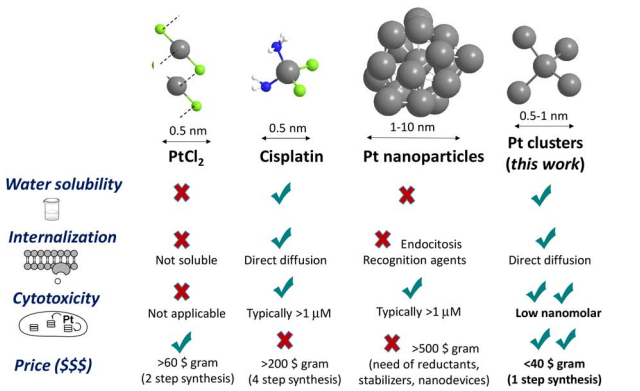

Fig. 1 Comparison of $PtCl_2$, cisplatin, Pt clusters and NPs. Some of the most relevant features of these Pt compounds for biomedical applications are shown. Prices are an average of different commercial sources in the year 2020, and the price for Pt clusters is calculated as an average of the starting material prices.

efficacy and simultaneously decrease toxicity. In this sense, the advent of nanoscience boosted studies on different types of Pt nanoparticles (NPs) as antitumoral agents, but the nanometer size of the particles seems to be inadequate for the internalization process by direct diffusion across the lipid bilayer.[6] This inherent drawback for NPs has only been overcome with functionalization strategies[7] and, for instance, nanodevices based on Pt NPs have shown great therapeutic success[8] when linked to easily recognizable and cell-degradable transport-facilitating modifiers such as PEGylated and polyamidoamine (PAMAM) tails. Thus, the search for alternative forms of Pt is continuously spurred,[9] in particular, for finding a Pt drug able to overcome cisplatin resistance in ovarian cancer. Incidentally, these studies have clearly unveiled that the smaller the Pt NP released into the inner cell the higher the antitumoral activity,[8b] not only because of better dynamics across the membrane but also because of a faster disaggregation of the Pt NPs within the cell, to give highly cytotoxic ligand-free aqueous Pt ions. Besides, ultrasmall nanoparticles are expected to have fewer adverse effects because of better renal clearance.[10] These precedents suggest that naked sub-nanometer platinum clusters (Pt NCs)[9a,b] may show a higher cytotoxic action by faster internalization, through direct diffusion across the cellular membrane.[11]

Hence, Pt clusters could be an appropriate material for delivering platinum inside tumour cells.[12–15] The cytotoxic activity of ligand-free Pt MCs has not been reported so far. Likewise, Pt MCs are intrinsically much more challenging to prepare than other metal clusters because metal agglomeration is favored by relativistic effects.[16] Apart from mass-selected synchrotron techniques[17] and some remarkable examples of solid surface stabilized Pt clusters,[18] biocompatible Pt clusters have only been prepared with complex dendrimer-encapsulated systems,[18b,19] which require a tedious synthetic approach with cell recognizable chemical links for endocytosis internalization. All these precedents severely limit the availability and biological applications of Pt; thus, it would be of high interest to investigate the ability of Pt MCs to induce cell death and their application in cancer therapy.

It is known that amide solvents (*N*-methyl formamide, *N*-methyl pyrrolidone,…) are able to generate Cu,[20] Pd,[21] Ag[22] and Au MCs[23] in solution by endogenous reduction of the corresponding metal salts and, in accordance, the amide polymer polyvinylpyrrolidone (PVP) is a particularly good solid support for generating and stabilizing very tiny ($\approx$1 nm) noble metal aggregates.[22a,24] This methodology has recently been modified by us with the bio- and water-compatible polymer EVOH, where an alcohol replaces an amide functionality as a mild reductant on a solid support, to generate metal clusters in organic solutions.[25] With this in mind, it was envisioned here that EVOH could generate MCs in water, and give neat MC aqueous solutions after cool filtration of the EVOH polymer. This approach will open the door for a cheap, general, biocompatible, and scalable synthesis of MCs in water, circumventing the toxicologic drawbacks associated with typical reductants, *i.e.*, amides or $NaBH_4$. The fact that Cu, Au, and Ag MCs, prepared by electrochemical methods in water, had shown significant biological activity,[22b] strongly suggests that other metal clusters could be also biologically active. With this background, here we report the multigram synthesis of ligand- and additive-free, sub-nanometer MCs of Pt in aqueous solutions, and assessment of cytotoxic activity towards several cell lines, including cisplatin-resistant tumor cells.

Results and discussion

Synthesis and characterization of aqueous metal clusters

Fig. 2 shows the synthesis and characterization of Pt clusters in water. The experimental procedure is extremely simple, and consists of treating a water/ethanol (1 : 1 v/v) solution of K_2PtCl_4 (1–10 μM) with the EVOH polymer at room temperature for 2 h, and filtering the polymer. Fig. 2a shows that the final material is a clear solution of Pt in water/ethanol, which is stable in a fridge for months, since the fluorescence spectra and the biological activity do not change during this time. The synthesis can be scaled up to 1 L of solution with the same final Pt content. For the sake of comparison, Pt clusters were prepared by a solid-phase procedure, dissolving EVOH at 75 °C, then adding K_2PtCl_4, and finally cooling to re-precipitate the polymer. The final material is, in this case, a solid film with the MCs directly embedded into the polymer.[25] Fig. 2b shows the UV-visible emission spectra of the Pt cluster aqueous solution (see also Fig. S1†) and Pt@EVOH (inset), where fluorescence signals can be clearly seen, with values that fit well with sub-nanometer Pt clusters according to the jellium model.[21] The corresponding absorption spectrum shows the absence of the typical atomic and plasmonic bands corresponding to K_2PtCl_4 and NPs (Fig. S2†). These results suggest that Pt clusters are generated in water after EVOH treatment at the expense of K_2PtCl_4, without significant formation of NPs, in agreement with the ability of clusters and the impossibility of single atoms and NPs to fluoresce.

Mass determination of the micromolar aqueous Pt clusters is extremely difficult by conventional techniques such as MALDI-TOF, since the concentration is well below the detection limit. However, we tried here to circumvent this drawback by using an Orbitrap analyser (HPLC-Orbitrap MS) with flow injection-high resolution mass spectrometry (HRMS). The use of an Orbitrap analyser was envisioned by virtue of its high sensitivity when operating in full scan mode and the valuable mass information provided, capable of determining low concentrations of analytes while allowing retrospective analysis. Its potential has been previously explored in the analysis of trace levels of organic contaminants,[26] but, to our knowledge, there are no applications involving metal clusters so far. As shown in Fig. 2c, the mass spectrum of the Pt clusters obtained using the Orbitrap revealed masses for Pt_3 hydroxide, oxide and chloride clusters, according to the *m*/*z* value, the isotopic Pt distribution and the recurrent loss of 16 a.u. fragments (oxygen atoms) when compared with the blank sample (Fig. S3†). Besides, the spectrum does not show any peak of the starting K_2PtCl_4.

Fig. 2d shows different aberration-corrected high angle annular dark field-scanning transmission electron images (AC-HAADF-STEM) of the Pt clusters in water, just deposited on the grid. The presence of MCs, as the major species, can be clearly

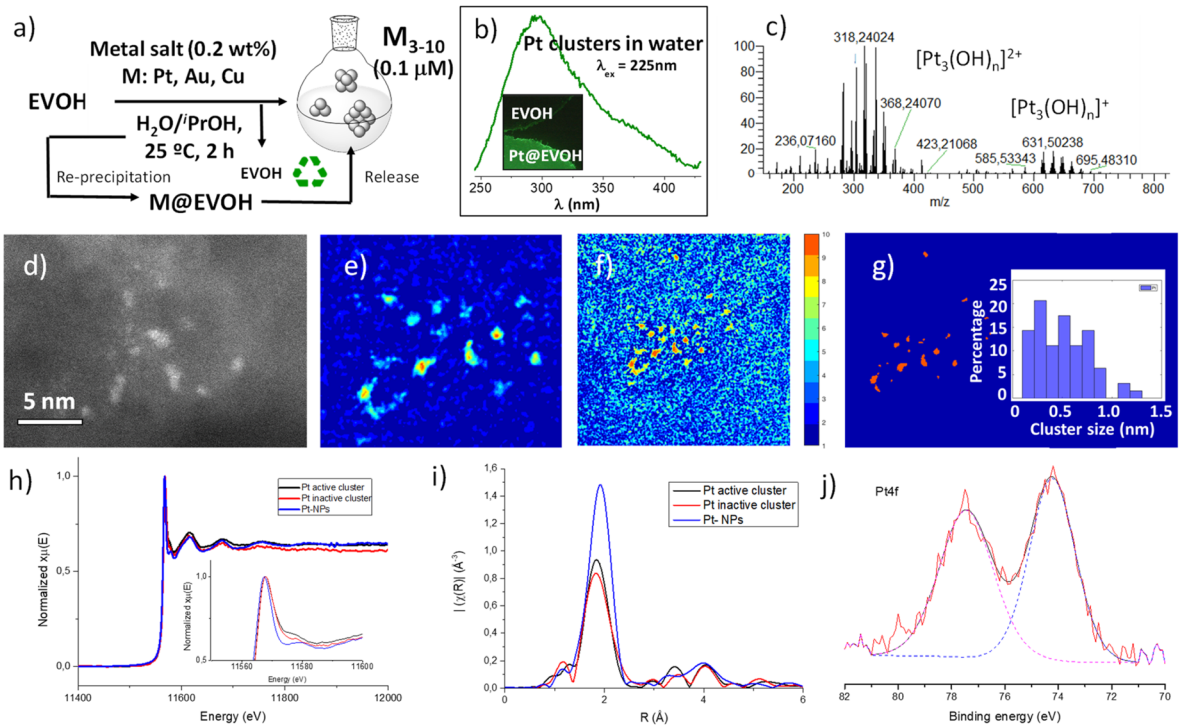

Fig. 2 Synthesis and characterization of Pt clusters in water. (a) Synthesis of clusters in water solution or embedded in EVOH. (b) Emission spectrum after irradiating the water solution with Pt clusters at 225 nm; the inset shows fluorescence microscopy of EVOH before and after incorporating Pt clusters within the solid (Pt@EVOH). (c) High-resolution mass spectrum of the Pt clusters in water, obtained using an ORBITRAP instrument. (d) AC HAADF-STEM image of the aqueous solution. (e) RGB image of the processed image of the Pt clusters after denoising and background subtraction. (f) κ-Means clustering method results for the experimental image. (g) Automatic identification of the subnanometer Pt species using segmentation by κ-means clustering with the corresponding cluster size distribution histogram. (h) X-ray absorption near edge structure (XANES). (i) Extended x-ray absorption fine structure (EXAFS). (j) X-ray photoelectron spectra (XPS) of Pt@EVOH. (k) AC HAADF-STEM image of the cluster aqueous solution adsorbed on charcoal (Pt@charcoal).

observed (see also Fig. S4 and S5†). Fig. 2e–g shows a denoised HAADF-STEM image with the corresponding κ-means clustering analysis.[27] The selection of the κ-means cluster number which corresponds to the Pt signal has allowed the image to be binarized, where Pt is displayed in orange and the background in blue. The Pt cluster size is estimated from these binarized images by calculating the equivalent diameter of the orange areas, considered as circles, providing a reliable histogram of the MC size distribution. The results unveil that *c.a.* 90% of the Pt particles are in the sub-nanometer range, with a Pt atomicity between 3 and 10, in accordance with the fluorescence measurements. The direct visualization of the MCs was complemented with X-ray absorption near edge structure (XANES) and extended X-ray absorption fine structure (EXAFS) spectra. Due to the detection limit of the detector and the low concentration of Pt in the MC water solutions, spectroscopic data have been collected on Pt@EVOH. Fig. 2h and i show that, these clusters are partially oxidized, as evidenced by the Orbitrap analyses. Pt foil and Pt (II) compounds were used to obtain a "white line" intensity *vs.* oxidation state calibration curve (Fig. S6†), since all the "white lines" at Pt L_3-edge peaks are quite sharp; thus, their energy position is simple to identify by looking at the derivative, and the Pt species analysed are surrounded by either oxygen or Pt atoms. With these standards in hand, the Pt clusters having between 3 and 10 atoms show an oxidation state of +0.66 (Fig. 2h), while a more oxidized but biologically inactive sample (*vide infra*) shows a slightly higher oxidation state (+0.82, Table S1†). The analysis of the EXAFS region (Fig. 2i) in the K range available fits with Pt–Pt and Pt–O–Pt bonds for the Pt clusters and the XPS spectra (Fig. 2j) is in good agreement with the XANES and EXAFS measurements, where all the Pt present in the cluster is partially oxidized (74.5 eV).

From the characterization above, we cannot discard the presence of some single Pt atoms and dimers, since the AC-HAADF-STEM histogram lists some <0.4 nm particles and the synchrotron measurements detect single atom Pt coordination spheres, but, oxidized MCs seem to be the major species, representing around 90% of the total species. In order to confirm this calculation, the Pt cluster aqueous solution was treated with activated charcoal, since a smaller size and a higher ionic charge-to-radius ratio of single Pt atoms and dimers with respect to MCs should favour the adsorption of the former on the negatively charged high surface area of charcoal, thus providing a method for separation and analysis. The results (Fig. S7†) showed the exclusive adsorption of Pt_1 and Pt_2 species on the charcoal surface, which accounted for *c.a.* 10% of the total Pt species in water. Thus, Pt MCs are the main species in both water solution and the solid, accounting for *ca.* 90% of the total Pt species. The latter highlights that the K_2PtCl_4 precursor

has reacted quantitatively, and that Pt single atoms and Pt NPs are not significantly formed during the aqueous synthesis.

Cellular cytotoxic activity of Pt clusters

Internalization of Pt clusters. Cellular uptake of the Pt MCs was first assessed in human cervix carcinoma (HeLa) cells using inductively coupled plasma atomic emission spectroscopy (ICP-AES) after incubation and cell lysis with a 10% Triton-100 solution and compared to cisplatin. Uptake standardisation was carried out according to the cell number seeded in each well, which was equal in each experiment (1.5×10^4 cells). The results showed that a significant amount of the metal was found in the lysates (305 μmol), which was 2.5-fold higher than cisplatin (120 μmol). To further check the presence of Pt MCs inside the cells, combined high-resolution transmission electron microscopy (HR-TEM) and AC-HAADF-STEM of osmium (Os) and uranyl (U) stained samples was carried out. Even though visualizing sub-nanometric Pt MCs in Os- and U-stained samples was unsuccessful, amorphous Pt oxide aggregates were found inside cells (Fig. 3a). Pt aggregates mainly displayed a cytoplasmic localization, and, noticeably, they were able to reach the nucleus. More details are provided in the ESI (Fig. S8 and S9†).

Cytotoxicity of Pt clusters. Afterward, the antiproliferative properties of Pt MCs were investigated using the colorimetric

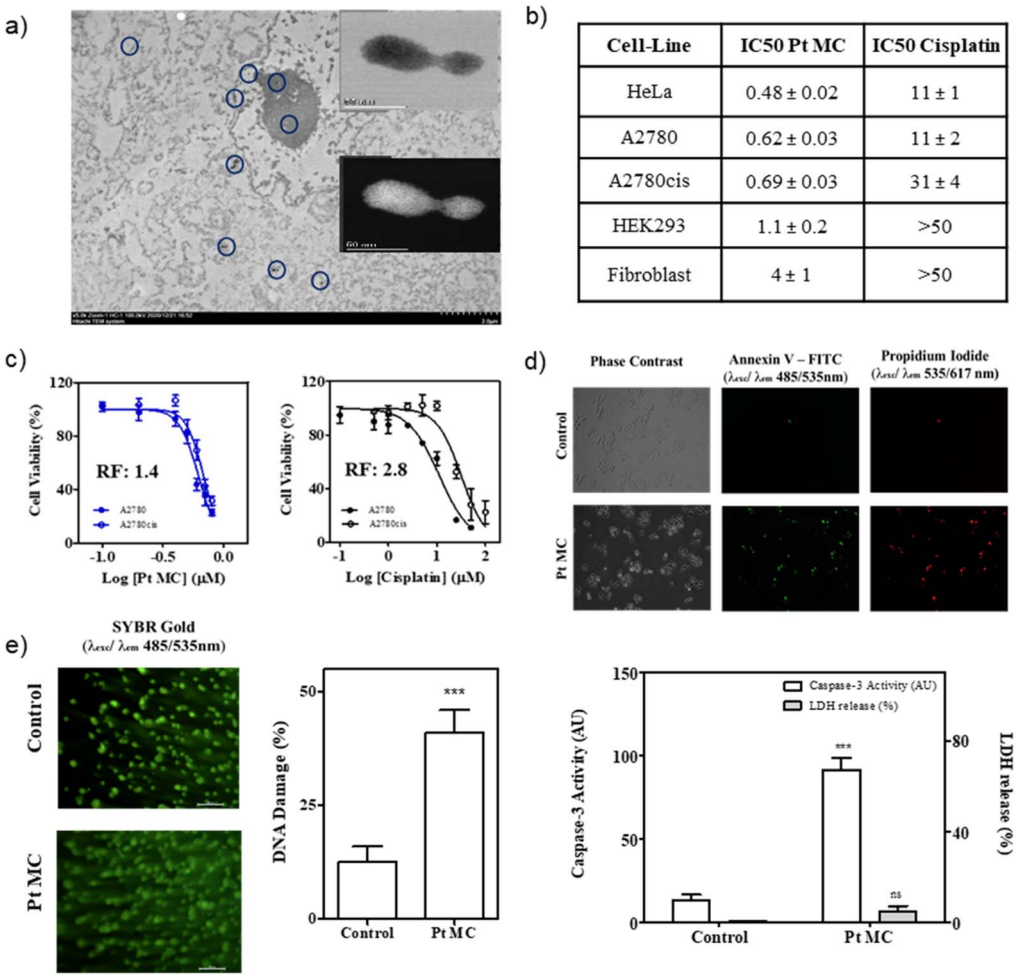

Fig. 3 Cytotoxicity activity of Pt metal clusters. (a) Cellular uptake of Pt MCs in HeLa cells. HR-TEM amorphous aggregations of Pt clusters circled in blue and inset: AC-HAADF-STEM images of a HeLa sample treated with Pt MCs. (b) Cytotoxicity of Pt MCs against tumoral and non-tumoral cell lines by MTT assay. Data are the mean ± SD of three dose-response independent experiments. Cisplatin (0.1–50 μM) was used as the standard compound. (c) Cytotoxicity profiles of Pt MCs (left) and cisplatin (right) including ovarian cancer cells (A2780) and cisplatin-resistant cells (A2780cis). (d) Top: Cell morphology and fluorescence microscopy images of annexin-V/propidium iodide double-staining of HeLa cells after treatment with Pt MCs. Cells were labelled with annexin-V-FITC ($\lambda_{exc}/\lambda_{em}$ 485/535 nm; green fluorescence) and propidium iodide ($\lambda_{exc}/\lambda_{em}$ 535/617 nm; red fluorescence) and visualized with a Leica fluorescence microscope PAULA. Bottom: Caspase-3 activation assay and LDH release by HeLa cells upon treatment with platinum metal clusters. Data are the mean ± SD of three independent dose-response experiments. Asterisks indicate the confidence degree of the measurements between groups by the student's *t*-test (***$p < 0.001$ ns: non-significant). (e) DNA damage induced by Pt MCs against HeLa cells by comet assay. Left: Fluorescence microscopy images (green fluorescence) of comet experiments. Cells were treated with PtMCs and incubated for 24 h. Images are representative of three independent experiments. Right: Quantitation of DNA damage by means of a 6-class visual classification score. Data represent the mean ± SD of three independent experiments. Asterisks indicate the confidence degree of the measurements between groups by the DNA damage (***$p < 0.001$).

MTT cell viability assay.[28] For this purpose, a panel of the human ovarian cancer cell line was selected: HeLa, A2780, and its cisplatin-resistant variant A2780cis. Thus, after 24 h treatment of the above-mentioned cells with an appropriate range of concentrations (0.05–10 μM, see the ESI† for further details), dose-response curves (Fig. S10†) were obtained to determine the IC_{50} values and they were compared with those obtained for cisplatin, which was used as a reference (Fig. 3b). The results point out an antiproliferative effect for the Pt MCs against HeLa and A2780 cells in the nanomolar range with an IC_{50} of 0.48 μM and 0.62 μM, respectively, which was *ca.* 20-fold lower than that for cisplatin ($IC_{50} = 11$ μM). Next, antiproliferative properties of Pt MCs were investigated in HeLa cells using a higher incubation period (48 h). However, no significant differences were found between the IC_{50} values obtained at both incubation periods. Hence, when the study was extended to other cell lines, attention was paid antiproliferative research at 24 h. In a further step, to determine the compound selectivity against tumoral cells, assays were conducted using non-tumoral cells HEK-293 and human fibroblasts. As a trend, Pt MCs displayed lower cytotoxicity against non-tumoral cells with a higher IC_{50} compared to tumoral cell lines. This effect was higher for human fibroblasts with an 8.3-fold higher IC_{50} value, thus suggesting that Pt MCs could be quite selective against tumoral cells.

Cisplatin drug resistance is significantly attributed to the loss of Pt internalization by active diffusion through the Cr1 Cu channels in resistant cells,[29] and since the internalization of the Pt clusters is expected to also occur by passive diffusion, it may be that the Pt clusters circumvent the Cr1 Cu resistant channels to kill cisplatin-resistant tumour cells, regardless of how the final DNA damage occurs.[30] To test this exciting hypothesis a new set of experiments were performed on the human ovarian cancer A2780 cell line and its cisplatin-resistant variant A2780cis. Fig. 3c shows that Pt clusters in water exhibited a nanomolar cytotoxic activity for cisplatin-resistant tumour cells, nearly similar to non-resistant cells ($IC_{50} = 0.68$ *vs.* 0.48 μM, respectively), with a resistance factor of just 1.4. This result is highly remarkable and provides a new strategy to treat cisplatin-resistant tumours beyond complex organometallic compounds or biomolecular systems.

To investigate whether the cytostatic properties displayed by Pt MCs could lead to cell death, cells treated for 24 h with the metal clusters were stained with annexin V-FITC/propidium iodide (AnnV/PI) and visualized using fluorescence microscopy. This assay detects phosphatidylserine translocation to the outer leaflet of the plasma membrane using recombinant annexin V conjugated with FITC (green-fluorescent dye) and membrane permeabilization with propidium iodide, giving red fluorescence. As shown in Fig. 3d, cells upon treatment with Pt MCs displayed mainly green and red fluorescence, indicative of late apoptotic cells or necrotic cells, whereas non-treated cells showed negligible fluorescence. Different apoptotic and necrotic cell death markers were further analyzed to explore the mechanism of Pt MC-induced cytotoxicity. In this sense, caspase-3 activity is usually considered a hallmark of apoptosis, whereas lactate dehydrogenase (LDH) release indicates compromised cell membranes, which is characteristic of necrotic cell death. The results displayed in Fig. 3d for both experiments indicate that Pt MC treatment induces significant activation of caspase-3, with non-significant LDH release to the medium, thus suggesting apoptosis as the underlying pathway promoting cell death by the clusters.

Genotoxic effects of Pt clusters. To understand whether the Pt MCs could induce alterations in the DNA molecule and therefore producing genotoxicity in cells, alkaline single-cell gel electrophoresis (comet) assay experiments were carried out. This test reveals different kinds of damage to the chromosomic DNA of an individual cell, such as single and double-strand breaks, incomplete excision repair sites and alkali-labile sites. Thus, as shown in Fig. 3e, exposure of cells to the metal clusters resulted in significant DNA damage in HeLa cells, as revealed by high DNA migration that moved faster through the agarose gel, forming a tail. By contrast, negligible DNA damage was observed upon Pt MC treatment in non-tumoral cells (Fig. S11†). In addition, the MCs are confirmed to be stable under-conditions mimicking intracellular conditions (Fig. S12†).

Rationalization of the cytotoxic activity of metal clusters

Computational calculations were performed in order to mimic the DNA damage imparted by this series of Pt compounds.[31] Our model systems are designed by locating an initial Pt center on the N7 guanine atom, which is the preferred site for DNA platination.[32]

The top panel of Fig. 4 shows that the equilibrium associated with the reaction of Pt_1–Pt_{10} MCs with guanine is largely shifted towards the adduct product, with interaction energies in the range of −38 and −59 kcal mol^{-1}. However, a dissimilar biological activity is expected depending on the cluster size. Indeed, even though the smallest clusters (Pt_1–Pt_4) can platinate DNA, MCs with 5–8 metallic centres might be optimal for inducing cellular damage, as they correlate with the strongest interaction with DNA (Fig. S13†). Not only that, the performed calculations predict the reactivity of partially oxidized clusters with the same atomicity of the parent MCs (Pt_xO_{x-1}, with $2 \leq x \leq 6$), since the smallest oxidized entities (*i.e.* Pt_2O and Pt_3O_2) produce adducts with a similar efficiency to those of the pure–Pt counterparts (Pt_3 and Pt_5, respectively). In contrast, larger oxidized forms (Pt_4O_3, Pt_5O_4 and Pt_6O_5) are associated with significantly more stable adducts (interaction energies of about −65 and −70 kcal mol^{-1}).

Aiming to gain a better understanding of such numeric values, the computational analysis is completed by monitoring the attack of the Pt species to guanine, which in turn allows for assessing the kinetics of the reaction. The most reactive oxidized clusters (*i.e.* Pt_6 and Pt_4O_3, respectively) are compared to cisplatin. Fig. 4 (bottom panel) illustrates that cisplatin leads to a more stable adduct with guanine with a predicted interaction energy of −87 kcal mol^{-1}. This observation agrees with that the formal 2+ positive charge on the metallic centre is concomitant with a larger interaction energy compared to MCs. However, theory demonstrates that cisplatin requires an early activation by hydrolysis of the chloride ligand, with an energetic

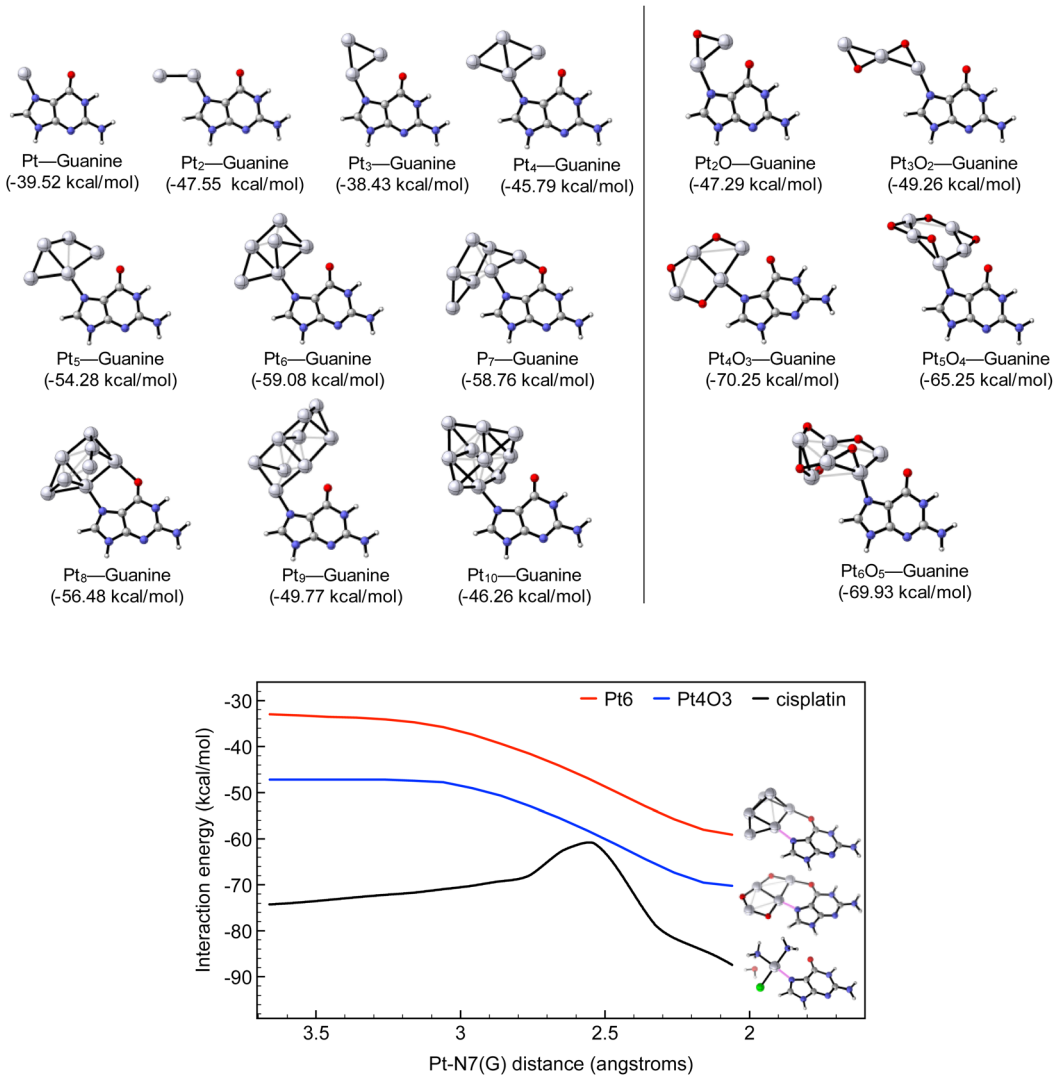

Fig. 4 Density-functional calculations. Optimized geometries of MC-guanine adducts as predicted by computational methods. Both precursor clusters (P_x-guanine left panel) and their oxidized counterparts (P_xO_{x-1}-guanine, right panel) have been assessed. Values in parenthesis indicate the computed complexation energies in kcal mol^{-1}. The used level of theory combines the M06 functional and the def2SVP basis set for all atoms, except Pt. For the latter, the def2-ECP basis set is used to account for relativistic effects. Color scheme: gray, C atoms; blue, N atoms; red, O atoms; dark blue, Pt atoms; white, H atoms. The graphic below shows the interaction energy profile (kcal mol^{-1}) for the reaction with a guanine base. All intermediate geometries are optimized by monitoring the distance between the reactive Pt center and the N7 site (distance is marked as a pink line and displayed in angstroms). Colour scheme: gray, C atoms; blue, N atoms; red, O atoms; green, Cl atom; white, H atoms. Pt atoms are displayed as larger gray balls.

barrier of 16.32 kcal mol^{-1}. In striking contrast, MCs do not need such activation by hydrolysis and react with DNA through a barrierless profile as MCs undergo *via* barrierless processes. All these accumulated numeric outputs suggest that the smallest MC (with an atomicity of up to 5) will be equally reactive with DNA; however, larger oxidized MCs are expected to induce more permanent damage to DNA compared to their raw precursors. In both cases, the reaction of MCs with DNA is kinetically favoured over cisplatin.

To check the feasibility of binding Pt clusters to a guanine base, analysis by MALDI-TOF evidenced new peaks at *m*/*z* 347, which corresponds to an increment of 151 a.m.u. and is related to the formation of an adduct (Pt-guanine), and at *m*/*z* 1045, which is compatible with protonated Pt_3-$(guanine)_3$ and loses one and two Pt atoms to give new peaks at *m*/*z* 850 and 655, respectively. These results further support the good correlation between the calculated energies for the formation of the adduct Pt-guanine and the experimental studies, regardless of how the final DNA damage occurs.[32]

Cisplatin is most probably the cheapest antitumoral metal drug in the market, despite an estimated price >200 € per gram.[4] The relatively high price of cisplatin comes from the four-step manufacturing method, which starts from K_2PtCl_4 and requires the use of expensive stoichiometric reagents such as $AgNO_3$. The aqueous Pt cluster synthesis starts from the same Pt precursor as cisplatin, *i.e.*, K_2PtCl_4, but requires just the cheap polymer EVOH as the only reagent and one synthetic step, which makes the price of the therapeutic Pt dramatically

lower. For the sake of illustration, Fig. 1 compares the most relevant characteristics of representative Pt compounds: $PtCl_2$,[33] cisplatin, Pt NPs and the Pt clusters synthesized in this work, and it can be seen there that the Pt clusters are not only much more active than cisplatin and Pt NPs, but their synthesis clearly simplifies and strikingly improves current Pt drugs, with an estimated price at least 5–10 times cheaper, nearly as simple as $PtCl_2$. Thus, the present study introduces not only fundamental but also synthetic and economic approaches to produce novel metal drugs for the treatment of ovarian cancer cell lines.

Synthesis of other potential cytotoxic MCs

The synthetic methodology for Pt MCs can be extended not only to PGM metals such as Rh and Ir, but also to Au and Cu, by also obtaining MC-supported solids (M@EVOH, M = Pt, Rh, Ir, Au, and Cu). The resulting materials can be stored at room temperature for longer-periods of at least two years, and serve comparative characterization purposes between MCs. The solid films can be used as a source of ligand-free aqueous MCs on demand, after releasing the MCs in water.[20a] The new MCs were characterized by combined spectrophotometric, mass spectrometric and electron microscopy measurements (Fig. S14–S18†). With these results in hand, one can say that sub-nanometer MCs of 3 to 10 atoms can be formed in water just by simple treatment of a metal salt with EVOH.

As shown in Fig. 5a, a significant amount of cell internalized metal was found for cisplatin compared to all the MCs tested. These results suggest that MCs act as a convenient shuttle for metal cell internalization, without the need of ligands or additives. Since the antitumoral activity only depends on the type of metal employed and not on the ligands or additive, different aqueous MCs can be used to fairly compare the intrinsic antitumoral activity between metals. Fig. 5a also shows the IC_{50} values obtained for the different metal compounds and, even though they have lower IC_{50} values, there is a remarkably higher activity for Rh and Ir MCs of 2.4 and 4.5 μM against HeLa tumour cells, respectively (see also Fig. S19†), compared with cisplatin (11 μM, see Fig. 3). These MCs are also stable under mimic conditions for intracellular conditions (Fig. S20†), and Fig. 5b shows that Rh MCs displayed a very similar cell death to Pt MCs at the IC_{50} concentrations. Fig. 5c shows that cell death occurs by apoptosis and not by necrosis, as revealed by the caspase-3 activity and LDH release experiments, respectively, which indicates that the Pt and Rh clusters specifically trigger the programmed death mechanism within the tumour cell. Overall, these results suggest that the Ir and Rh MCs also require special attention as promising new antitumor agents.[34] Despite having the highest cell uptake of the MCs tested, Au clusters showed a very low cytotoxicity ($IC_{50} \geq 40$ μM), which indicates that Au metal is intrinsically less cytotoxic than Pt, Rh and Ir. To further test this hypothesis, not only Pt but also Au and Cu, both metals associated with a low cytotoxicity, were prepared in the form of different clusters by an electrochemical method[35] and also with PAMAM as a ligand (Fig. S21–S25†),[36] and tested in the MTT assay. However, cell proliferative analysis (Fig. S26†) and dose-response viability curves (Fig. S27†) with HeLa cells showed that the IC_{50} value was very high for all PAMAM-MCs, regardless of the synthetic method or size, which showcases the relevance

a)

MCs	[ ] internalized (μmol)[a]	IC50 (μM)[b]
Rh MC	150	4.5 ± 0.5
Ir MC	162	2.4 ± 0.2
Au MC	900	> 40

[a] quantified by ICP-MS
[b] analyzed by the MTT assay upon 24 h treatment with MCs

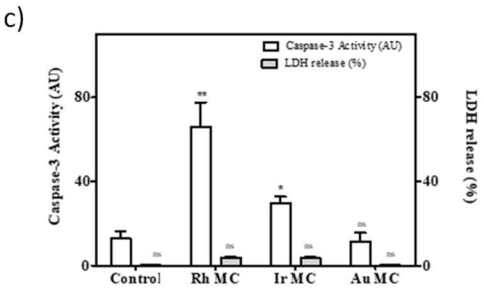

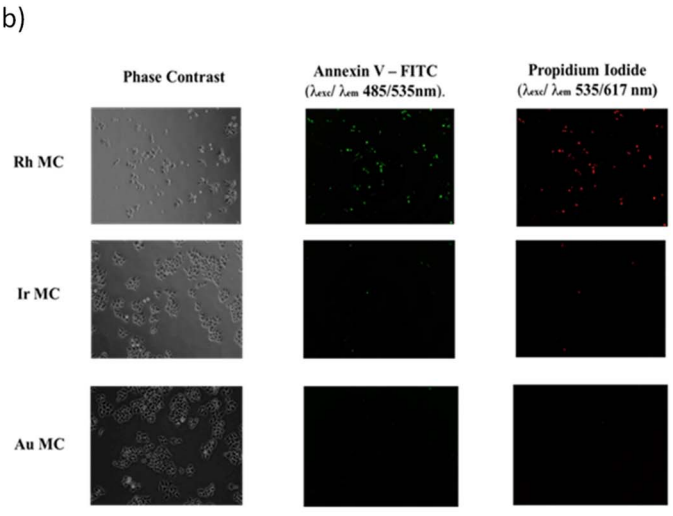

Fig. 5 Antitumoral activity of metal clusters. (a) Table with the results from cellular internalization and IC_{50} values of metal clusters in the HeLa cell line. Uptake standarisation was performed according to the cell number seeded (1.5×10^4 cell per well) for each condition. (b) Cell morphology and fluorescence microscopy images of annexin-V/propidium iodide double-staining of HeLa cells after treatment with metal clusters. Cells were labelled with annexin-V-FITC ($\lambda_{exc}/\lambda_{em}$ 485/535 nm; green fluorescence) and propidium iodide ($\lambda_{exc}/\lambda_{em}$ 535/617 nm; red fluorescence) and visualized with the Leica fluorescence microscope PAULA. (c) Caspase-3 activation assay and LDH release by HeLa cells upon treatment with metal clusters. Data are the mean ± SD of three independent dose-response experiments. The arterisks indicate the confidence degree of the measurements comparing them with untreated cells (control) by the *t*-Student test (***$p < 0.001$, **$p < 0.01$, *$p < 0.05$; ns: non-significant).

for the antitumoral activity of the ligand-free form of MCs. The stability of the naked MCs in solution without stabilizing agents comes from the high dilution, as assessed by fluorescence measurements at increasing concentrations of Pt, where the rapid disappearance of the Pt MC fluorescence at higher concentrations can be observed (Fig. S28†).

Conclusions

Sub-nanometer additive-free aqueous clusters of Pt, Rh and Ir have been prepared in one step from the corresponding metal salts, allowing the comparison of the intrinsic cytotoxicity of the metals. Thus, Pt MCs show an extremely high cytotoxic activity (in the nM range) toward cancer cell lines, including cisplatin-resistant cells. Moreover, Pt MCs reveal DNA damage through the comet experiments. Experimental and computational studies indicate that the high cytotoxicity of the Pt clusters could be ascribed to their unique structure and atomicity, which allow an enhanced internalization within cells. All these findings point to MCs as promising potential candidates for cancer therapy and open new avenues in the search for new antitumoral metal drugs.[37]

Author contributions

R. G. performed the synthesis, characterization and catalytic experiments of the MCs in water; G. G.-L. performed and analysed data for cell tests; J. O.-M. and C. M. designed, performed and interpreted the synchrotron experiments; I. D. performed and analysed the Orbitrap results; M. L.-H. and J. C. H.-G. carried out the HR STEM measurements, image analysis and simulations; J. P. C.-C. designed, performed and interpreted the DFT calculations; I. A. conceived and supervised the biological assays, guided interpretation of the cytotoxicity part, and wrote the manuscript; A. L.-P. conceived and coordinated the work, supervised the synthetic part, and wrote the manuscript.

Conflicts of interest

There are no conflicts to declare.

Acknowledgements

This work was supported by MINECO (Spain, Projects CTQ 2017-86735-P [AEI/FEDER, UE], PID2020-115010RB-I00, BEAGAL 18/00211, MAT2017-87579-R, IJC2018-036514-I and SEV-2016-0683). Financial support by the project PID2020-115100GB-I00 (funded by Spanish MCIINN, MCIN/AEI/10.13039/501100011033MICIIN) is acknowledged. STEM studies were performed at the DME-UCA node of the National Unique Infrastructure for Electron Microscopy of Materials, ELECMI. Theoretical calculations were conducted in the Poznan Supercomputing Center and in the Plataforma Andaluza de Bioinformática located at the Universidad Málaga, Spain. The proteomic analysis was performed in the proteomics facility of the SCSIE University of Valencia. We gratefully acknowledge ALBA synchrotron for allocating beamtime and CLÆSS beamline staff for their technical support during our experiment. R. G. thanks ITQ for the concession of a contract. We also thank M. T. Mínguez-Hernández (SCSIE, UV) for the preparation of ultramicrotome samples.

Notes and references

1 S. Lheureux, C. Gourley, I. Vergote and A. M. Oza, *Lancet*, 2019, **393**, 1240.

2 Z. Momenimovahed, A. Tiznobaik, S. Taheri and H. Salehiniya, *Int. J. Womens Health*, 2019, **11**, 287.

3 (*a*) P. Liu, L. Zhao, J. Pol, S. Levesque, A. Petrazzuolo, C. Pfirschke, C. Engblom, S. Rickelt, T. Yamazaki, K. Iribarren, L. Senovilla, L. Bezu, E. Vacchelli, V. Sica, A. Melis, T. Martin, L. Xia, H. Yang, Q. Li, J. Chen, S. Durand, F. Aprahamian, D. Lefevre, S. Broutin, A. Paci, A. Bongers, V. Minard-Colin, E. Tartour, L. Zitvogel, L. Apetoh, Y. Ma, M. J. Pittet, O. Kepp and G. Kroemer, *Nat. Commun.*, 2019, **10**, 1486; (*b*) C. Segovia, E. San José-Enériz, E. Munera-Maravilla, M. Martínez-Fernández, L. Garate, E. Miranda, A. Vilas-Zornoza, I. Lodewijk, C. Rubio, C. Segrelles, L. V. Valcárcel, O. Rabal, N. Casares, A. Bernardini, C. S. Cabrera, F. F. L. Calderón, P. Fortes, J. A. Casado, M. Dueñas, F. Villacampa, J. J. Lasarte, F. G. Ramos, G. de Velasco, J. Oyarzabal, D. Castellano, X. Agirre, F. Prósper and J. M. Paramio, *Nat. Med.*, 2019, **25**, 1073.

4 S. Ghosh, *Bioorg. Chem.*, 2019, **88**, 102925.

5 (*a*) L. Qi, Q. Luo, Y. Zhang, F. Jia, Y. Zhao and F. Wang, *Chem. Res. Toxicol.*, 2019, **32**, 1469; (*b*) J. Huang, J. Li, Y. Lyu, Q. Miao and K. Pu, *Nat. Mater.*, 2019, **18**, 1133; (*c*) A. Casado-Sánchez, C. Martín-Santos, J. M. Padrón, J. M. Padrón, R. Mas-Ballesté, C. Navarro-Ranninger, J. Alemán and S. Cabrera, *J. Inorg. Biochem.*, 2017, **174**, 111; (*d*) F. Navas, F. Mendes, I. Santos, C. Navarro-Ranninger, S. Cabrera and A. G. Quiroga, *Inorg. Chem.*, 2017, **56**, 6175; (*e*) T. C. Johnstone, K. Suntharalingam and S. J. Lippard, *Chem. Rev.*, 2016, **116**, 3436; (*f*) Z. H. Siddik, *Oncogene*, 2003, **22**, 7265.

6 (*a*) S. Ashraf, A. Hassan Said, R. Hartmann, M.-A. Assmann, N. Feliu, P. Lenz and W. J. Parak, *Angew. Chem., Int. Ed.*, 2020, **59**, 5438; (*b*) S. Sindhwani, A. M. Syed, J. Ngai, B. R. Kingston, L. Maiorino, J. Rothschild, P. MacMillan, Y. Zhang, N. U. Rajesh, T. Hoang, J. L. Y. Wu, S. Wilhelm, A. Zilman, S. Gadde, A. Sulaiman, B. Ouyang, Z. Lin, L. Wang, M. Egeblad and W. C. W. Chan, *Nat. Mater.*, 2020, **19**, 566; (*c*) C. Zhang, L. Yan, Z. Gu and Y. Zhao, *Chem. Sci.*, 2019, **10**, 6932.

7 (*a*) I. Abánades Lázaro, S. Haddad, S. Sacca, C. Orellana-Tavra, D. Fairen-Jimenez and R. S. Forgan, *Chem*, 2017, **2**, 561; (*b*) D. Kim, K. Shin, S. G. Kwon and T. Hyeon, *Adv. Mater.*, 2018, **30**, 1802309.

8 (*a*) H. Xia, F. Li, X. Hu, W. Park, S. Wang, Y. Jang, Y. Du, S. Baik, S. Cho, T. Kang, D.-H. Kim, D. Ling, K. M. Hui and T. Hyeon, *ACS Cent. Sci.*, 2016, **2**, 802; (*b*) H.-J. Li, J.-Z. Du, X.-J. Du, C.-F. Xu, C.-Y. Sun, H.-X. Wang, Z.-T. Cao, X.-Z. Yang, Y.-H. Zhu, S. Nie and J. Wang, *Proc. Natl. Acad. Sci.*, 2016, **113**, 4164.

9 (*a*) O. Domarco, C. Kieler, C. Pirker, C. Dinhof, B. Englinger, J. M. Reisecker, G. Timelthaler, M. D. García, C. Peinador, B. K. Keppler, W. Berger and A. Terenzi, *Angew. Chem., Int. Ed.*, 2019, **58**, 8007; (*b*) A. Eskandari, A. Kundu, S. Ghosh and K. Suntharalingam, *Angew. Chem., Int. Ed.*, 2019, **58**, 12059; (*c*) Z. Deng, N. Wang, Y. Liu, Z. Xu, Z. Wang, T.-C. Lau and G. Zhu, *J. Am. Chem. Soc.*, 2020, **142**, 7803; (*d*) Z. Wang, Z. Deng and G. Zhu, *Dalton Trans.*, 2019, **48**, 2536; (*e*) D. Veclani, A. Melchior, M. Tolazzi and J. P. Cerón-Carrasco, *J. Am. Chem. Soc.*, 2018, **140**, 14024; (*f*) X. Xue, M. D. Hall, Q. Zhang, P. C. Wang, M. M. Gottesman and X.-J. Liang, *ACS Nano*, 2013, **7**, 10452.

10 C. N. Loynachan, A. P. Soleimany, J. S. Dudani, Y. Lin, A. Najer, A. Bekdemir, Q. Chen, S. N. Bhatia and M. M. Stevens, *Nat. Nanotechnol.*, 2019, **14**, 883.

11 (*a*) D. Chen, S. Gao, W. Ge, Q. Li, H. Jiang and X. Wang, *RSC Adv.*, 2014, **4**, 40141; (*b*) Y. Yamagishi, A. Watari, Y. Hayata, X. Li, M. Kondoh, Y. Yoshioka, Y. Tsutsumi and K. Yagi, *Nanoscale Res. Lett.*, 2013, **8**, 395.

12 (*a*) M. Boronat, A. Leyva-Pérez and A. Corma, *Acc. Chem. Res.*, 2014, **47**, 834; (*b*) J. Oliver-Meseguer, J. R. Cabrero-Antonino, I. Domínguez, A. Leyva-Pérez and A. Corma, *Science*, 2012, **338**, 1452.

13 A. Corma, P. Concepción, M. Boronat, M. J. Sabater, J. Navas, M. J. Yacaman, E. Larios, A. Posadas, M. A. López-Quintela, D. Buceta, E. Mendoza, G. Guilera and A. Mayoral, *Nat. Chem.*, 2013, **5**, 775.

14 E. C. Tyo and S. Vajda, *Nat. Nanotechnol.*, 2015, **10**, 577.

15 D. Buceta, N. Busto, G. Barone, J. M. Leal, F. Domínguez, L. J. Giovanetti, F. G. Requejo, B. García and M. A. López-Quintela, *Angew. Chem., Int. Ed.*, 2015, **54**, 7612.

16 (*a*) A. Leyva-Pérez and A. Corma, *Angew. Chem., Int. Ed.*, 2012, **51**, 614; (*b*) J. Lee, J. Yang, S. G. Kwon and T. Hyeon, *Nat. Rev. Mater.*, 2016, **1**, 16034.

17 S. Vajda, M. J. Pellin, J. P. Greeley, C. L. Marshall, L. A. Curtiss, G. A. Ballentine, J. W. Elam, S. Catillon-Mucherie, P. C. Redfern, F. Mehmood and P. Zapol, *Nat. Mater.*, 2009, **8**, 213.

18 (*a*) M. Mon, M. A. Rivero-Crespo, J. Ferrando-Soria, A. Vidal-Moya, M. Boronat, A. Leyva-Pérez, A. Corma, J. C. Hernández-Garrido, M. López-Haro, J. J. Calvino, G. Ragazzon, A. Credi, D. Armentano and E. Pardo, *Angew. Chem., Int. Ed.*, 2018, **57**, 6186; (*b*) T. Imaoka, Y. Akanuma, N. Haruta, S. Tsuchiya, K. Ishihara, T. Okayasu, W.-J. Chun, M. Takahashi and K. Yamamoto, *Nat. Commun.*, 2017, **8**, 688; (*c*) O. Guillén-Villafuerte, G. García, B. Anula, E. Pastor, M. C. Blanco, M. A. López-Quintela, A. Hernández-Creus and G. A. Planes, *Angew. Chem., Int. Ed.*, 2006, **45**, 4266.

19 Y. Li, J. H.-C. Liu, C. A. Witham, W. Huang, M. A. Marcus, S. C. Fakra, P. Alayoglu, Z. Zhu, C. M. Thompson, A. Arjun, K. Lee, E. Gross, F. D. Toste and G. A. Somorjai, *J. Am. Chem. Soc.*, 2011, **133**, 13527.

20 (*a*) J. Oliver-Messeguer, L. Liu, S. García-García, C. Canós-Giménez, I. Domínguez, R. Gavara, A. Doménech-Carbó, P. Concepción, A. Leyva-Pérez and A. Corma, *J. Am. Chem. Soc.*, 2015, **137**, 3894; (*b*) P. Maity, S. Yamazoe and T. Tsukuda, *ACS Catal.*, 2013, **3**, 182.

21 A. Leyva-Pérez, J. Oliver-Meseguer, P. Rubio-Marqués and A. Corma, *Angew. Chem., Int. Ed.*, 2013, **52**, 11554.

22 (*a*) I. Pastoriza-Santos and L. M. Liz-Marzán, *Langmuir*, 2002, **18**, 2888; (*b*) B. Santiago-Gonzalez, A. Monguzzi, M. Caputo, C. Villa, M. Prato, C. Santambrogio, Y. Torrente, F. Meinardi and S. Brovelli, *Sci. Rep.*, 2017, **7**, 5976.

23 H. Kawasaki, H. Yamamoto, H. Fujimori, R. Arakawa, Y. Iwasaki and M. Inada, *Langmuir*, 2010, **26**, 5926.

24 P. Maity, S. Takano, S. Yamazoe, T. Wakabayashi and T. Tsukuda, *J. Am. Chem. Soc.*, 2013, **135**, 9450.

25 E. Fernández, M. A. Rivero-Crespo, I. Domínguez, P. Rubio-Marqués, J. Oliver-Meseguer, L. Liu, M. Cabrero-Antonino, R. Gavara, J. C. Hernández-Garrido, M. Boronat, A. Leyva-Pérez and A. Corma, *J. Am. Chem. Soc.*, 2019, **141**, 1928.

26 I. Domínguez, F. J. Arrebola, J. L. Martínez Vidal and A. Garrido Frenich, *J. Chromatogr. A*, 2020, **1619**, 460964.

27 L. Liu, M. Lopez-Haro, C. W. Lopes, C. Li, P. Concepcion, L. Simonelli, J. J. Calvino and A. Corma, *Nat. Mater.*, 2019, **18**, 866.

28 P. W. Sylvester, *Methods Mol. Biol.*, 2011, **716**, 157.

29 S. Ishida, J. Lee, D. J. Thiele and I. Herskowitz, *Proc. Natl. Acad. Sci. U. S. A.*, 2002, **99**, 14298.

30 (*a*) W. Yu, R. Liu, Y. Zhou and H. Gao, *ACS Cent. Sci.*, 2020, **6**, 100; (*b*) K. S. Egorova and V. P. Ananikov, *Angew. Chem., Int. Ed.*, 2016, **55**, 12150.

31 (*a*) E. R. Jamieson and S. J. Lippard, *Chem. Rev.*, 1999, **99**, 2467; (*b*) M. Kartalou and J. M Essigmann, *Mutat. Res.*, 2001, **478**, 1.

32 (*a*) J. V. Burda, J. Šponer, J. Hrabáková, M. Zeizinger and J. Leszczynski, *J. Phys. Chem. B*, 2003, **107**, 5349; (*b*) A. S. Chaves, M. J. Piotrowski and J. L. F. Da Silva, *Phys. Chem. Chem. Phys.*, 2017, **19**, 15484.

33 P. Rubio-Marqués, M. A. Rivero-Crespo, A. Leyva-Pérez and A. Corma, *J. Am. Chem. Soc.*, 2015, **137**, 11832.

34 (*a*) J. M. Bailis, A. G. Weidmann, N. F. Mariano and J. K. Barton, *Proc. Natl. Acad. Sci. U. S. A.*, 2017, **114**, 6948; (*b*) J. J. Conesa, A. C. Carrasco, V. Rodríguez-Fanjul, Y. Yang, J. L. Carrascosa, P. Cloetens, E. Pereiro and A. M. Pizarro, *Angew. Chem., Int. Ed.*, 2020, **59**, 1270; (*c*) A. Okrut, R. C. Runnebaum, X. Ouyang, J. Lu, C. Aydin, S.-J. Hwang, S. Zhang, O. A. Olatunji-Ojo, K. A. Durkin, D. A. Dixon, B. C. Gates and A. Katz, *Nat. Nanotechnol.*, 2014, **9**, 459; (*d*) D. L. Ma, D. S. Chan and C. H. Leung, *Acc. Chem. Res.*, 2014, **47**, 3614.

35 M. J. Rodríguez-Vázquez, M. C. Blanco, R. Lourido, C. Vázquez-Vázquez, E. Pastor, G. A. Planes, J. Rivas and M. A. López-Quintela, *Langmuir*, 2008, **24**, 12690.

36 (*a*) T. Imaoka, H. Kitazawa, W.-J. Chun and K. Yamamoto, *Angew. Chem., Int. Ed.*, 2015, **54**, 9810; (*b*) H. Ye and R. M. Crooks, *J. Am. Chem. Soc.*, 2005, **127**, 4930.

37 (*a*) Q. Xu, Y. Pan, X. Liu, Y. Gao, X. Luan, F. Zeng, D. Zhou, W. Long, Y. Wang and Y. Song, *Angew. Chem., Int. Ed.*, 2022, **61**, e202114239; (*b*) A. Barba-Bon, G. Salluce, I. Lostalé-Seijo, K. I. Assaf, A. Hennig, J. Montenegro and W. M. Nau, *Nature*, 2022, **603**, 637.